NIH Public Access
Author Manuscript
J Biomol NMR. Author manuscript; available in PMC 2014 August 06.

Published in final edited form as:
J Biomol NMR. 2011 April ; 49(0): 175–184. doi:10.1007/s10858-011-9491-7.

A metabolomic comparison of mouse models of the Neuronal Ceroid Lipofuscinoses

Reza M. Salek,
Department of Biochemistry and the Cambridge Systems Biology Centre, University of Cambridge, 80 Tennis Court Road, Cambridge, CB2 1GA, UK

Michael R. Pears,
Department of Biochemistry and the Cambridge Systems Biology Centre, University of Cambridge, 80 Tennis Court Road, Cambridge, CB2 1GA, UK

Jonathan D. Cooper,
Pediatric Storage Disorders Laboratory, Department of Neuroscience, Institute of Psychiatry, King's College London, London, UK

Hannah M. Mitchison,
Department of Paediatrics and Child Health, Royal Free and University College Medical School, London, UK

David A. Pearce,
Department of Pediatrics, Sanford School of Medicine of the University of South Dakota, 2301 East 60th Street North, Sioux Falls, SD 57104-0589, USA

Russell J. Mortishire-Smith, and
Johnson & Johnson PR & D, Turnhoutsweg 30, 2340 Beerse, Belgium

Julian L. Griffin
Department of Biochemistry and the Cambridge Systems Biology Centre, University of Cambridge, 80 Tennis Court Road, Cambridge, CB2 1GA, UK. Department of Biochemistry, University of Cambridge, Building O, Downing Site, Tennis Court Road, Cambridge CB2 1QW, UK

Julian L. Griffin: jlg40@mole.bio.cam.ac.uk

Abstract

The Neuronal Ceroid Lipofuscinoses (NCL) are a group of fatal inherited neurodegenerative diseases in humans distinguished by a common clinical pathology, characterized by the accumulation of storage body material in cells and gross brain atrophy. In this study, metabolic changes in three NCL mouse models were examined looking for pathways correlated with neurodegeneration. Two mouse models; motor neuron degeneration (*mnd*) mouse and a variant model of late infantile NCL, termed the neuronal ceroid lipofuscinosis (*nclf*) mouse were investigated experimentally. Both models exhibit a characteristic accumulation of autofluorescent

© Springer Science+Business Media B.V. 2011
Correspondence to: Julian L. Griffin, jlg40@mole.bio.cam.ac.uk.

NIH-PA Author Manuscript
NIH-PA Author Manuscript
NIH-PA Author Manuscript

NIH-PA Author Manuscript

NIH-PA Author Manuscript

NIH-PA Author Manuscript

lipopigment in neuronal and non neuronal cells. The NMR profiles derived from extracts of the cortex and cerebellum from *mnd* and *nclf* mice were distinguished according to disease/wildtype status. In particular, a perturbation in glutamine and glutamate metabolism, and a decrease in γ-amino butyric acid (GABA) in the cerebellum and cortices of *mnd* (adolescent mice) and *nclf* mice relative to wildtype at all ages were detected. Our results were compared to the *Cln3* mouse model of NCL. The metabolism of *mnd* mice resembled older (6 month) *Cln3* mice, where the disease is relatively advanced, while the metabolism of *nclf* mice was more akin to younger (1–2 months) *Cln3* mice, where the disease is in its early stages of progression. Overall, our results allowed the identification of metabolic traits common to all NCL subtypes for the three animal models.

Keywords

Juvenile Neuronal Ceroid Lipofuscinosis (JNCL); Batten disease; CLN3; NMR; Metabolomics; Neurodegeneration

Introduction

The NCLs are a family of genetically inherited metabolic storage diseases which exhibits a common pathology, manifesting lysosomal accumulation of autofluorescent lipopigment, neurodegeneration and premature death (Mann et al. 1978; Sekhon and Maxwell 1974). The hallmark of the symptoms of the NCLs is impaired vision, mental and motor deterioration often accompanied by ataxia, myoclonus and epilepsy. Traditional diagnosis of NCL gave rise to ‘classical’ NCL subtypes known as: infantile (CLN1), late infantile (CLN2), juvenile (CLN3) and adult (CLN4). Subsequent advances in genetic analyses led to the recognition of four additional NCL subtypes (Goebel and Sharp 1998), variants of the classical late infantile form (CLN2) and mutations in genes designated *CLN5*, *CLN6*, *CLN7* and *CLN8*. The corresponding CLN3 protein is targeted to the lysosomes in non-neuronal cells (Jarvela et al. 1998; Kyttala et al. 2004), but is also localized to the presynaptic terminals and synaptosomes in primary neuronal cells (Luiro et al. 2001). The function of CLN3 has been analyzed in two yeast models, and is associated with vacuole function (Gachet et al. 2005; Kim et al. 2003; Pearce et al. 1999). In addition, mammalian studies have suggested a role for CLN3 in cytoskeletal function and membrane trafficking (Luiro et al. 2004).

The *Cln3* mouse constitutes a model of juvenile NCL (Batten disease) whereby the mouse *Cln3* gene, having 82% sequence identity (Lee et al. 1996) with human *Cln3*, has been disrupted. Evidence for metabolic dysfunction related to arginine metabolism in $Cln3^{-/-}$ mouse has been previously reported (Chan et al. 2009), as well as similar changes detected in a yeast model (Kim et al. 2003), and in lymphoblasts from patient cell lines bearing mutations in CLN3 (Ramirez-Montealegre and Pearce 2005). Studies carried out on $Cln3^{-/-}$ mice have also demonstrated disruption in the citrulline-Nitric oxide cycle (Chan et al. 2009).

Previously using metabolomic based techniques we demonstrated an increased concentration of glutamine and decreased concentrations of glutamate, N-acetyl aspartate and GABA in $Cln3^{-/-}$ mice (Pears et al. 2005). The reduction in the concentration of GABA appeared to

NIH-PA Author Manuscript

NIH-PA Author Manuscript

NIH-PA Author Manuscript

parallel the loss of specific GABAergic inter-neurons reported in affected brains (Oswald et al. 2001), as well as suggesting changes in glutamate/glutamine/GABA cycling.

In addition to the *Cln3*$^{-/-}$ mouse there is a naturally occurring mouse mutant called the motor neuron degeneration (*mnd*) mouse, containing a one base pair insertion in the orthologous mouse *Cln8* gene (82% homologous to human gene) resulting in a frame shift defect (Ranta et al. 1999). These mice have been shown to exhibit abnormalities akin to those in human NCL patients. Specifically, autofluorescent inclusions in interneuron, the retina and in many somatic organs (Bronson et al. 1998; Pardo et al. 1994). In addition, retinal degeneration is pronounced at 1 month of age with widespread loss of photoreceptor and retinal cells (Chang et al. 1994). Neurological and motor changes have also been documented in the *mnd* mouse with profound cortical atrophy which is apparent at 9 months of age with progressive loss of hippocampal and cortical GABAergic evident from 5 months of age (Cooper et al. 1999). Up regulation of glial fibrillary acidic protein (GFAP) occurred at 9 months of age, indicative of reactive gliosis. In addition we have previously shown that glutamate/glutamine cycling is altered in these mice (Griffin et al. 2002).

The neuronal ceroid lipofuscinosis (*nclf*) mouse is a model of late infantile NCL (Bronson et al. 1998). *nclf* mouse contain a one base pair insertion in the orthologous mouse *Cln6* gene (90% homologous to human gene) resulting in a frame shift defect (Wheeler et al. 2002). Similar to the *mnd* mouse, *nclf* mouse exhibit a characteristic accumulation of autofluorescent lipopigment in neuronal and non neuronal cells. Cortical atrophy, progressive loss of hippocampal and cortical GABAergic interneurons and the development of cerebral gliosis have all been documented in *nclf* mice (Bronson et al. 1998; Mitchison et al. 1999). However, these mice have been shown to have a more protracted clinical course than *mnd* mice, exhibiting comparable symptoms but with a delay of ~2 months. For example, *nclf* mice are clinically normal until 8 months of age, at which time they develop spastic rear limb paresis which progresses to paralysis and eventually death by 12 months (Bronson et al. 1998).

Relative to the *Cln3* mice, *mnd* and *nclf* mice display more profound morphological defects. Motor deterioration occurs much earlier with onsets of 4 and 8 months in *mnd* and *nclf* mice, respectively, compared to *Cln3* mice where there is no obvious motor dysfunction until 16 months of age. Furthermore, retinal function is not compromised in *Cln3* mice. It may be that the different genetic background of the *Cln3* mouse (129S6) affects the penetrance of the mutation, making it difficult to make direct comparisons. Alternatively, the delayed phenotype of the *Cln3* mouse may simply represent the more protracted clinical course of juvenile NCL (Batten disease). Indeed, another *Cln3* knockout mouse, on a C57BL/6J background, also exhibits NCL like pathologies later than those in *mnd* and *nclf* mice (Katz et al. 1999). Here, we have implemented metabolomic techniques to investigate metabolite profiles in cortex and cerebellum brain regions of the *mnd* and the *nclf* mice, both exhibiting abnormalities akin to those in human NCL patients, and compared these changes with results found in the *Cln3* mouse.

NIH-PA Author Manuscript

NIH-PA Author Manuscript

NIH-PA Author Manuscript

Materials and methods

Mice sample collection

Tissue from wildtype, *mnd* (Chang et al. 1994) and *nclf* (Bronson et al. 1998) mice on a C57/BL background were taken from stable mouse colonies at Rochester University, NY, USA (Table 1). Colonies were housed in micro isolator cages on Lab diet 5010 (PMI Nutritional International, Brentwood, MO, USA) under a strict 12 h light/dark cycle, at 22°C with a relative humidity of 70–75%. Tissue was taken rapidly (within 30 s) after sacrifice by cervical dislocation, snap-frozen in liquid nitrogen and stored at −80°C. All procedures conformed to the National Institutes of Health guidelines and the University of Rochester Animal Care and Use Committee Guidelines. The cortex and cerebellum (20–50 mg wet weight) were dissected on ice and the individual samples stored in micro-centrifuge tubes at −80 °C.

Extraction and preparation of aqueous metabolites

Frozen cortex and cerebellum brain tissue samples (~50 and 20 mg, respectively) were ground on dry ice using a pestle and mortar, and methanol and chloroform in a ratio of 2:1 (v/v; 1 ml) added (Le Belle et al. 2002). Homogenates were sonicated for 15 min, after which 200 μl each of chloroform and distilled water were added. The phases were separated by centrifugation, and the upper aqueous phase was removed and dried in an evacuated centrifuge (Eppendorf, Hamburg, Germany). Subsequently, the dried tissue extracts were reconstituted in 600 μl of 50 mM sodium phosphate buffer in D_2O (pH 7.4), which contained 0.25 mM sodium (3-trimethylsilyl)-2,2,3,3-tetra-deuteriopropionate (TSP) (Cambridge Isotope Laboratories, Inc, USA) as a chemical shift standard, and placed into 5 mm NMR tubes (Wilmad-Lab Glass, New Jersey, USA).

1D ^{1}H NMR data acquisition

One-dimensional spectra were acquired using a conventional pre-saturation pulse sequence for water suppression based on the first increment of the nuclear Overhauser effect spectroscopy (NOESY) pulse program (relaxation delay-90°-t_1-90°-t_m-90°-acquire) (Macura and Huang 1981), whereby the water resonance was irradiated during the relaxation delay. Spectra for C57BL/6J control, *mnd* and *nclf* mice aged 6 months were recorded on DRX500 Bruker (Bruker BioSpin GmbH, Rheinstetten, Germany) at a proton frequency of 500 MHz at 27°C (relaxation delay = 1.3 s, mixing time of t_m = 150 ms, t_1 = 3 s). Samples were analyzed using 3 mm NMR tubes, 196 scans with a spectral width of 12.00 ppm. For the C57BL/6J control, *mnd* and *nclf* mice aged 9 and above spectra were recorded on a Bruker Avance III spectrometer, equipped with a 5 mm TXI ATMA probe (Bruker BioSpin GmbH, Rheinstetten, Germany) using 5 mm tubes at a proton frequency of 500.3 MHz, temperature of 27°C (relaxation delay = 2.0 s, t_m = 50 ms, with t_1 fixed at 4 μs). Each spectrum was acquired with 128 scans collected into 64 k data points with an acquisition time of 4.09 s and spectral width of 16.00 ppm.

All spectra were processed using 1D NMR Manager software (Advanced Chemistry Development Inc., Toronto, Canada). Spectra were multiplied by an exponential weighting function corresponding to a line broadening of 0.3 Hz and Fourier transformed from the time

NIH-PA Author Manuscript

NIH-PA Author Manuscript

NIH-PA Author Manuscript

to the frequency domain. Spectra were phased, baseline corrected and referenced to the TSP singlet at 0.00 ppm. Spectra were segmented into 0.04 ppm chemical shift bins between 0.2 and 9.8 ppm (excluding water and TSP resonances) using a fixed bucket size of 0.04 and the Intelligent Bucketing facility within ACD NMR Manager (projection method and 50% looseness factor implemented). To account for differences in sample volumes, each integrated region was normalised to the total spectral area for all integral regions in that spectrum, excluding water and TSP resonances. Spectra were assigned by comparison with assignment tables (Lindon et al. 1999; Govindaraju et al. 2000; Pears et al. 2005; Salek et al. 2008; Salek et al. 2010) and on-line databases (http://www.bmrb.wisc.edu/metabolomics and http://mmcd.nmrfam.wisc.edu) such that metabolites contributing to each bin were defined.

Chemometric analyses

Multivariate data analysis was carried out using SIMCA-P + 12.0 (Umetrics AB, Umeå, Sweden) with the data mean centred and Pareto scaled prior to analysis. Pareto scaling augments the representation of low concentration metabolites in statistical models by dividing each integral region or variable by the square root of the standard deviation of the variable, without increasing the contribution spectral noise makes to the model. Three different multivariate statistical techniques were used within the SIMCA package; principal components analysis (PCA) and projection to latent structures by partial least squares discriminant analysis (PLS-DA) and Orthogonal PLS-DA (OPLS-DA). PCA is an unsupervised technique that describes observations (i.e. spectra from mouse brain tissue) with regards to one or more latent variables termed principal components (PCs) which are linear combinations of the original variables (NMR buckets). PLS-DA and OPLS are supervised techniques separating observations based on class-membership. In OPLS-DA the objective is to remove the variation in the model that is orthogonal to response and this can produce more easily interpretable models where the first component represents the major changes that distinguish the two groups (Trygg and Wold 2002). The weights given to each original NMR variable within any given principle component describe how influential that particular variable is and the relation (or correlation) of the variables to each other. To determine which of the original variables are responsible for this separation the loading scores and correlation coefficients of the loadings for each model was analysed (Jackson 1991; Wold et al. 1984). The first component of the loading plots was plotted against NMR chemical shifts to complement the scores plot. The coefficient values were multiplied by a factor to represent both their contribution to the loadings scores and their significance. The significance of the contribution was determined by multiplying (1-*p*-value) against the coefficient. The p-value itself was calculated using a Student's *t* test on the coefficients for a jack-knifing routine used to calculate the contribution from each variable made to a given component. The parameters R^2 and Q^2 were used to evaluate the performance of each model. The R^2 score indicates how much of the total variation in the dataset is described by a particular component and R^2_{cum} indicates the variation described by all the components in the model. Q^2 estimates the predictive ability of the model by leaving out observations (1/7th) from the building of the model and then predicting their class membership or trend variable. All PLS-DA and OPLS-DA models were assessed for the risk of being spurious

NIH-PA Author Manuscript

NIH-PA Author Manuscript

NIH-PA Author Manuscript

i.e., the model fits the training set well but does not accurately predict Y for new observations (Eriksson et al. 1999) using the validate function within the SIMCA package.

Results

A metabolomics approach was used to define biochemical abnormalities associated with two mouse models of NCL subtypes, *mnd* and *nclf* mice, associated with late variant infantile NCL (CLN8) and CLN6 NCL subtypes, respectively. Our objective was to acquire metabolic changes across two NCL subtypes at different ages and to compare the above models to the previously described *Cln3* mouse model (Pears et al. 2005). The ^{1}H NMR spectral profiles from the cortex (Fig. 1) and cerebellum of wildtype, *mnd* and *nclf* mice were examined for metabolic abnormalities.

Young (6 months) mnd and nclf mice both exhibit distinct cerebral metabolic profiles relative to control mice

Wildtype and *mnd* ^{1}H NMR spectral profiles were readily separated by PLS-DA when the cortex and cerebellum brain regions were considered separately (Fig. 2a, b). Analysis of the variable coefficients for these models identified several metabolic perturbations responsible for each separation (Table 2). Lactate, glutamine, choline, phosphocholine (PC) and glycerophosphocholine (GPC) were increased in concentration in *mnd* cortex and cerebellum tissues relative to wildtype, whilst creatine, γ-aminobutyric acid (GABA), taurine and *myo*-inositol were decreased. In addition, N-acetyl aspartate (NAA) and aspartate were decreased in the *mnd* cortex relative to wildtype, whilst isoleucine/valine/leucine, *scyllo*-inositol and ethanolamine were increased in the cortex. Glutamate was increased in the cortex, but decreased in the cerebellum.

Similarly, wildtype and *nclf* ^{1}H NMR profiles (mice aged 6 months) were separated by PLS-DA when the cortex and cerebellum were considered separately (Fig. 2c, d) and several metabolic changes identified (Table 2). In the *nclf* mice, glutamate, glutamine, succinate, aspartate and NAA were increased in the cortex, while lactate, glutamine and aspartate were relatively increased in the cerebellum compared to wildtype. In both the cortex and cerebellum, choline/PC, GPC, creatine, *myo*-inositol and GABA were decreased in *nclf* mice relative to wildtype. In addition glutamate and taurine were also decreased in the cerebellum.

^{1}H NMR profiles from *mnd*, *nclf* and control mice were examined together to identify metabolite changes dominant for each mouse model. Separation, by PLS-DA between wildtype, *mnd* and *nclf* profiles was apparent in the cortex (Fig. 3a, with the relevant loading and validation plot shown in Fig. 3b–c) and cerebellum (Data not shown). In the cortex model, PLS component 1 described the variation associated with mouse strain while PLS component 2 represented disease associated variation common to both *mnd* and *nclf* mice. Analysis of component 1 and 2 loadings, revealed glutamine, glutamate and NAA were relatively increased in the *nclf* mouse cortex whereas creatine, GABA and taurine were increased in wildtype controls. Additionally choline/PC, aspartate and *myo*-inositol were relative increased in the *mnd* mice compared to the wild-type and *nclf* mice. An OPLS-DA model (Fig. 3d) combining both models of NCL against the control mice revealed common

NIH-PA Author Manuscript

NIH-PA Author Manuscript

NIH-PA Author Manuscript

metabolic traits. The metabolic changes were an increase in glutamate, glutamine and NAA while GABA, creatine and *myo*-inositol decreased in the mouse models of NCL.

The PLS-DA model for extracts of the cerebellum from wildtype, *mnd* and *nclf* mice was less predictable than the model for the cortex (Q^2 of 30% compared with 69%; data not shown). The disease effect dominated component 1, which separated mainly the wildtype mice from the two mouse models of NCL, while component 2 mainly separated the *mnd* from *nclf* mice. An OPLS-DA model comparing the combined grouping of the two NCL mouse models against their wildtype controls (Fig. 3e) highlighted metabolites contributing to the disease separation; these were relative increases in lactate, glutamate and glutamine and decreases in creatine, NAA, *myo*-inositol, taurine and GABA in the cerebellum of mutant mice. Adding the *Cln3* age matched data set and its control group to the dataset, and building a PLS-DA model for the young mice allowed the separation of the *mnd*, *nclf* and their wildtype (C57BL background) mice from *Cln3* and its wildtype mice (sv129 background) along component 1 (Fig. 3f). The separation along component 1 was mostly associated with strain difference while component 2 separated wildtype from the *Cln3* mice as well as *mnd* from *nclf* and control mice. Analysis of the loading plot and correlation coefficients of the loading (data not shown) indicated that lactate was increased in the sv129 wildtype, GABA, NAA, *myo*-inositol and glutathione in the *Cln3* mice, glutamate and taurine in the *nclf* mice and glutamine, creatine and choline/PC were increased in the *mnd* mice. However, in this model there was no clear separation between the wildtype (C57BL background) and the *nclf* mice.

The changes in the relative concentrations of GABA, NAA, glutamate and glutamine identified by the multivariate statistics were considered as ratios of GABA/Glu, Gln/Glu and NAA/Glu for the cortex (Table 3). The Gln/Glu ratio was decreased for all models of NCL compared to the wildtype, with changes being more significant for the *mnd* and *Cln3* mouse models. However, the ratios of GABA/Glu and NAA/Glu were only significantly different in the *mnd* and *Cln3* mouse models.

Metabolic changes in older nclf mice (18 months)

The young *nclf* group (6 month) for both the cortex and cerebellum spectra were readily separated from the spectra for the 9 and 18 months old animals. Studying the correlation coefficient of variables (data not shown) for the PLS-DA model of 9 versus 18 months old *nclf* mice identified several metabolites relevant to the difference associated with aging in mice. The mice aged 18 month had relatively decreased concentrations of taurine and GABA and increased concentrations of NAA, aspartate, *myo*-inositol and creatine compared to mice at 9 months. The cortex of the *nclf mice* at 18 months compared to wildtype (19 months) had increased concentrations of choline/PC, GPC and glutamate while glutamine, leucine, isoleucine and valine were decreased (Fig. 4a–b). The cerebellum of 18 month wildtype mice were also separated from the aged match *nclf* mice by PCA and PLS-DA analysis. Taurine, glutamate, leucine/isoleucine and valine were increased while choline/PC, GPC, *myo*-inositol, *scyllo*-inositol, GABA, aspartate and creatine were decreased in the *nclf* mice compared to wildtype (Fig. 4c). For the *mnd* mice aged 6 months and the *nclf* mice

NIH-PA Author Manuscript

NIH-PA Author Manuscript

NIH-PA Author Manuscript

aged 9 months the *n* number was not sufficient (*n* = 4—Table 1) to produce reliable and valid models.

Discussion

The systematic analysis of several NCL mouse models, encompassing an array of NCL subtypes, has enabled the definition of a catalogue of neuropathological landmarks for each NCL subtype (Cooper 2003). It is apparent that many of these mice share several degenerative features, including regional atrophy and loss of specific interneuronal populations in the cortex and hippocampus (Bible et al. 2004; Cooper 2003; Cooper et al. 1999; Mitchison et al. 2004; Pontikis et al. 2004). In this study, the metabolomic analysis using ^{1}H NMR spectroscopy of the *mnd* and *nclf* mouse models, in addition to the *Cln3* mouse, has enabled a comparative study of these models in terms of their metabolism in the cortex and cerebellum.

Similar metabolic traits were apparent in each NCL mouse model suggesting a common metabolic trend. In particular, glutamate was increased and GABA, creatine and *myo*-inositol were decreased in the cortices of *mnd* and *nclf* mice relative to wildtype. These changes were defined in models considering *mnd* and *nclf* profiles individually, as well in a model where the profiles were combined and analysed. Other metabolic changes were different between the two mouse models; choline and phosphocholine were decreased in the cortex of *nclf* mice and NAA and aspartate concentrations were decreased in the *mnd* mice. Further changes were observed which were specific to the individual mouse models. Therefore, while common metabolic trends were apparent between models of different NCL subtypes, unique metabolic perturbations also existed.

The cerebellum tissue from each NCL model was less predictable for genotype than the cortex which suggests that the cerebellum suffers a less severe phenotype than the cortex brain regions, in keeping with what is observed histologically. Metabolite changes identified in the cerebellum of both NCL models were similar to the cortex and included a relative increase in glutamine and lactate whilst glutamate, creatine, *myo*-inositol, GABA and taurine were decreased relative to wildtype. The differences between the NCL models included an increased choline/PC and GPC concentrations in *mnd* mice whereas the latter was reduced in young *nclf* but increased as mice aged. A similar increase in choline metabolites was also reported in the *Cln3* mice cortex (Pears et al. 2005). While a direct comparison between the *Cln3* mouse and the other two models is confounded by differences in strain backgrounds, the changes in phosphocholine are common across all three models. This in turn is suggestive of deregulated phospholipid metabolism. Perturbed phospholipid metabolism has also been previously documented in both infantile and juvenile NCL patients (Kakela et al. 2003). In addition, in the cortex of the aged *nclf* mice, the relative concentration of glutamine changed from being increased to decreased compared with wildtype controls. These changes detected in the aged *nclf* cortex are similar to that found in the *mnd* and *Cln3* mice. Other changes in the cerebellum of older *nclf* mice are an increase in glutamate and taurine and a decrease in aspartate in contrast to the young *nclf* mice. One caveat of the results from older *nclf* mice is that it was not possible to get perfectly matched aged controls at 18 months due to the complications and costs associated with breeding aged

NIH-PA Author Manuscript

NIH-PA Author Manuscript

NIH-PA Author Manuscript

mice. However, both the wildtype and *nclf* transgenic mice would be classed as aged mice and we would expect only minor changes as the mice aged from 18 to 19 months.

A decrease in GABA was observed in all NCL models. It has previously been suggested that the decrease in concentration of GABA detected in *Cln3* mice is due to the inhibitive action of autoantibodies for glutamic acid decarboxylase (GAD65) without compensation by the second GAD isoform, GAD76 (Pears et al. 2005; Chattopadhyay et al. 2002). However, such autoantibodies have not been detected in *mnd* and *nclf* mice. Therefore, given that all the mouse models display a loss of GABAergic neurons, it is likely that the decrease in GABA, at least in *mnd* and *nclf* mice, is reflective of GABAergic neuronal cell loss (Bronson et al. 1998; Cooper et al. 1999; Mitchison et al. 1999; Pontikis et al. 2004).

Changes in glutamate and glutamine metabolism were apparent in all NCL models. Collective changes in glutamate, glutamine and GABA are suggestive of a neurotransmitter cycling perturbation, as has been previously proposed in the *Cln3* mouse (Pears et al. 2005). Given that such cycling impairments have been observed in other neurological disorders, including epilepsy and Huntington's disease (Behrens et al. 2002; Burbaeva et al. 2003; Petroff et al. 2002), it is not surprising that this is a common trait across a range of NCL subtypes. Dysfunction of neurotransmitter cycling is likely to have a significant impact on the underlying NCL pathophysiology. The increase in glutamate concentration relative to GABA is consistent with, and extends the temporal scope of, a previous investigation, which revealed a similar increase in glutamate concentration at 3 months of age (Chattopadhyay et al. 2002). Since glutamate is the principle excitatory neurotransmitter, if this increased glutamate accumulates extracellularly it may result in increased stimulation of specific neurons leading to excitotoxicity. From an overall comparison of the cortex of mouse models of NCL, we detected that the highest perturbation in glutamate and glutamine metabolism was in the aged *nclf* and *mnd* mice as well as the largest perturbation in choline metabolism being found in *mnd* mice.

The metabolic profiles (Tables 2, 3) of *mnd* mice were more akin to older *Cln3* mice where the disease is relatively advanced, with an increase in choline/PC, glutamate and glutamine and decreases in the ratio of glutamine to glutamate, GABA, taurine and NAA (cortex only), relative to wildtype. Conversely, *nclf* mice were more akin to younger *Cln3* mice where the disease is in its early stages of progression (Table 3). These mice had an increase in glutamate and NAA within the cortex, and a decrease in GABA and choline/PC. This is consistent with *mnd* mice having an earlier clinical onset than *nclf* mice (Bronson et al. 1998; Chang et al. 1994). NAA has been suggested to be a precursor in myelin production by oligodendrocytes, providing a link between NAA degradation, lipid metabolism/transport, and metabolism within glia cells (Chakraborty et al. 2001). A decrease in the concentration of NAA in *mnd* mice suggest a potential impaired transportation of NAA from the mitochondrial production site to where it is metabolized. In addition, reductions in NAA have been linked to neuronal cell loss or thought to reflect changes in energy status of neurones in a number of neurodegenerative disorders. In addition, the PLS-DA model built using *mnd, nclf, Cln3* and their matched wildtype mice showed the *nclf* metabolic profile was most similar to that of control mice (close proximity of the clusters) suggesting a metabolic profile closer to that of wildtype rather than the *mnd* mice.

NIH-PA Author Manuscript

NIH-PA Author Manuscript

NIH-PA Author Manuscript

The results for the *mnd* mouse extend the temporal scope of a previous ^{1}H NMR metabolomic investigation, where the metabolic deficits associated with *mnd* mice aged 6 months were defined (Griffin et al. 2002). Glutamate was found to be increased, and glutamine and GABA decreased, in *mnd* mice relative to wildtype. Whilst a decrease in GABA concentration is consistent with the results of the current study, changes in glutamate and glutamine conflict. This may be because of differences in age as the relative proportions of glutamate and glutamine vary markedly with age as in *Cln3* mice (Pears et al. 2005).

Using a solution state ^{1}H NMR based metabolomic approach, profound metabolic changes have been identified in specific brain regions of *mnd* and *nclf* mice. Moreover, a comparative analysis of three NCL mouse models has enabled metabolic similarities and differences to be extracted. In the brain of the effected animal, a common metabolic trait comprises changes in glutamate, glutamine and GABA that is suggestive of impaired neurotransmitter cycling.

Acknowledgments

The authors would like to thank Dr. ChunHung Chan for help preparing the mice. This work was partially supported by Merck Sharp Dohme, NIH R21NS060185, NIH R21DK070288-01 and the Batten Disease Support and Research Association.

References

Behrens PF, Franz P, Woodman B, Lindenberg KS, Landwehrmeyer GB. Impaired glutamate transport and glutamate-glutamine cycling: downstream effects of the Huntington mutation. Brain. 2002; 125(Pt 8):1908–1922. [PubMed: 12135980]

Bible E, Gupta P, Hofmann SL, Cooper JD. Regional and cellular neuropathology in the palmitoyl protein thioesterase-1 null mutant mouse model of infantile neuronal ceroid lipofuscinosis. Neurobiol Dis. 2004; 16(2):346–359. [PubMed: 15193291]

Bronson RT, Donahue LR, Johnson KR, Tanner A, Lane PW, Faust JR. Neuronal ceroid lipofuscinosis (nclf), a new disorder of the mouse linked to chromosome 9. Am J Med Genet. 1998; 77(4):289–297. [PubMed: 9600738]

Burbaeva G, Boksha IS, Turishcheva MS, Vorobyeva EA, Savushkina OK, Tereshkina EB. Glutamine synthetase and glutamate dehydrogenase in the prefrontal cortex of patients with schizophrenia. Prog Neuropsychopharmacol Biol Psychiatry. 2003; 27(4):675–680. [PubMed: 12787856]

Chakraborty G, Mekala P, Yahya D, Wu G, Ledeen RW. Intraneuronal N-acetylaspartate supplies acetyl groups for myelin lipid synthesis: evidence for myelin-associated aspartoacylase. J Neurochem. 2001; 78(4):736–745. [PubMed: 11520894]

Chan CH, Ramirez-Montealegre D, Pearce DA. Altered arginine metabolism in the central nervous system (CNS) of the Cln3(−/−) mouse model of juvenile Batten disease. Neuropath Appl Neuro. 2009; 35(2):189–207.

Chang B, Bronson RT, Hawes NL, Roderick TH, Peng C, Hageman GS, Heckenlively JR. Retinal degeneration in motor neuron degeneration: a mouse model of ceroid lipofuscinosis. Invest Ophthalmol Vis Sci. 1994; 35(3):1071–1076. [PubMed: 8125718]

Chattopadhyay S, Ito M, Cooper JD, Brooks AI, Curran TM, Powers JM, Pearce DA. An autoantibody inhibitory to glutamic acid decarboxylase in the neurodegenerative disorder Batten disease. Hum Mol Genet. 2002; 11(12):1421–1431. [PubMed: 12023984]

Cooper JD. Progress towards understanding the neurobiology of Batten disease or neuronal ceroid lipofuscinosis. Curr Opin Neurol. 2003; 16(2):121–128. [PubMed: 12644737]

Cooper JD, Messer A, Feng AK, Chua-Couzens J, Mobley WC. Apparent loss and hypertrophy of interneurons in a mouse model of neuronal ceroid lipofuscinosis: evidence for partial response to insulin-like growth factor-1 treatment. J Neurosci. 1999; 19(7):2556–2567. [PubMed: 10087069]

NIH-PA Author Manuscript

NIH-PA Author Manuscript

NIH-PA Author Manuscript

Eriksson, L.; Johansson, E.; Kettaneh-Wold, N.; Wold, S. Introduction to multi- and megavariate data analysis using projection methods (PCA and PLS). Umetrics; Umea: 1999.

Gachet Y, Codlin S, Hyams JS, Mole SE. btn1, the Schizosaccharomyces pombe homologue of the human Batten disease gene CLN3, regulates vacuole homeostasis. J Cell Sci. 2005; 118(Pt 23): 5525–5536. [PubMed: 16291725]

Goebel HH, Sharp JD. The neuronal ceroid-lipofuscinoses. Recent advances. Brain Pathol. 1998; 8(1): 151–162. [PubMed: 9458173]

Govindaraju V, Young K, Maudsley AA. Proton NMR chemical shifts and coupling constants for brain metabolites. NMR Biomed. 2000; 13(3):129–153. [PubMed: 10861994]

Griffin JL, Muller D, Woograsingh R, Jowatt V, Hindmarsh A, Nicholson JK, Martin JE. Vitamin E deficiency and metabolic deficits in neuronal ceroid lipofuscinosis described by bioinformatics. Physiol Genomics. 2002; 11(3):195–203. [PubMed: 12388797]

Jackson, JE. A user's guide to principal components. Wiley; New York: 1991.

Jarvela I, Sainio M, Rantamaki T, Olkkonen VM, Carpen O, Peltonen L, Jalanko A. Biosynthesis and intracellular targeting of the CLN3 protein defective in Batten disease. Hum Mol Genet. 1998; 7(1):85–90. [PubMed: 9384607]

Kakela R, Somerharju P, Tyynela J. Analysis of phospholipid molecular species in brains from patients with infantile and juvenile neuronal-ceroid lipofuscinosis using liquid chromatography-electrospray ionization mass spectrometry. J Neurochem. 2003; 84(5):1051–1065. [PubMed: 12603829]

Katz ML, Shibuya H, Liu PC, Kaur S, Gao CL, Johnson GS. A mouse gene knockout model for juvenile ceroid-lipofuscinosis (Batten disease). J Neurosci Res. 1999; 57(4):551–556. [PubMed: 10440905]

Kim Y, Ramirez-Montealegre D, Pearce DA. A role in vacuolar arginine transport for yeast Btn1p and for human CLN3, the protein defective in Batten disease. Proc Natl Acad Sci USA. 2003; 100(26): 15458–15462. [PubMed: 14660799]

Kyttala A, Ihrke G, Vesa J, Schell MJ, Luzio JP. Two motifs target Batten disease protein CLN3 to lysosomes in transfected nonneuronal and neuronal cells. Mol Biol Cell. 2004; 15(3):1313–1323. [PubMed: 14699076]

Le Belle JE, Harris NG, Williams SR, Bhakoo KK. A comparison of cell and tissue extraction techniques using high-resolution 1H-NMR spectroscopy. NMR Biomed. 2002; 15(1):37–44. [PubMed: 11840551]

Lee RL, Johnson KR, Lerner TJ. Isolation and chromosomal mapping of a mouse homolog of the Batten disease gene CLN3. Genomics. 1996; 35(3):617–619. [PubMed: 8812504]

Lindon JC, Nicholson JK, Everett JR. NMR spectroscopy of biofluids. Annual Reports on Nmr Spectroscopy. 1999; 38:1–88.

Luiro K, Kopra O, Lehtovirta M, Jalanko A. CLN3 protein is targeted to neuronal synapses but excluded from synaptic vesicles: new clues to Batten disease. Hum Mol Genet. 2001; 10(19): 2123–2131. [PubMed: 11590129]

Luiro K, Yliannala K, Ahtiainen L, Maunu H, Jarvela I, Kyttala A, Jalanko A. Interconnections of CLN3, Hook1 and Rab proteins link Batten disease to defects in the endocytic pathway. Hum Mol Genet. 2004; 13(23):3017–3027. [PubMed: 15471887]

Macura S, Huang Y. Two-dimensional chemical exchange and cross-relaxation spectroscopy of coupled nuclear spins. J Magn Reson. 1981; 43(2):259–281.

Mann DM, Yates PO, Stamp JE. The relationship between lipofuscin pigment and ageing in the human nervous system. J Neurol Sci. 1978; 37(1–2):83–93. [PubMed: 690665]

Mitchison HM, Bernard DJ, Greene ND, Cooper JD, Junaid MA, Pullarkat RK, de Vos N, Breuning MH, Owens JW, Mobley WC, Gardiner RM, Lake BD, Taschner PE, Nussbaum RL. Targeted disruption of the Cln3 gene provides a mouse model for Batten disease. The Batten Mouse Model Consortium [corrected]. Neurobiol Dis. 1999; 6(5):321–334. [PubMed: 10527801]

Mitchison HM, Lim MJ, Cooper JD. Selectivity and types of cell death in the neuronal ceroid lipofuscinoses. Brain Pathol. 2004; 14(1):86–96. [PubMed: 14997941]

NIH-PA Author Manuscript

NIH-PA Author Manuscript

NIH-PA Author Manuscript

Oswald MJ, Kay GW, Palmer DN. Changes in GABAergic neuron distribution in situ and in neuron cultures in ovine (OCL6) Batten disease. Eur J Paediatr Neurol. 2001; 5(Suppl A):135–142. [PubMed: 11588985]

Pardo CA, Rabin BA, Palmer DN, Price DL. Accumulation of the adenosine triphosphate synthase subunit C in the mnd mutant mouse. A model for neuronal ceroid lipofuscinosis. Am J Pathol. 1994; 144(4):829–835. [PubMed: 8160780]

Pearce DA, Ferea T, Nosel SA, Das B, Sherman F. Action of BTN1, the yeast orthologue of the gene mutated in Batten disease. Nat Genet. 1999; 22(1):55–58. [PubMed: 10319861]

Pears MR, Cooper JD, Mitchison HM, Mortishire-Smith RJ, Pearce DA, Griffin JL. High resolution 1H NMR-based metabolomics indicates a neurotransmitter cycling deficit in cerebral tissue from a mouse model of Batten disease. J Biol Chem. 2005; 280(52):42508–42514. [PubMed: 16239221]

Petroff OA, Errante LD, Rothman DL, Kim JH, Spencer DD. Glutamate-glutamine cycling in the epileptic human hippocampus. Epilepsia. 2002; 43(7):703–710. [PubMed: 12102672]

Pontikis CC, Cella CV, Parihar N, Lim MJ, Chakrabarti S, Mitchison HM, Mobley WC, Rezaie P, Pearce DA, Cooper JD. Late onset neurodegeneration in the Cln3−/− mouse model of juvenile neuronal ceroid lipofuscinosis is preceded by low level glial activation. Brain Res. 2004; 1023(2): 231–242. [PubMed: 15374749]

Ramirez-Montealegre D, Pearce DA. Defective lysosomal arginine transport in juvenile Batten disease. Hum Mol Genet. 2005; 14(23):3759–3773. [PubMed: 16251196]

Ranta S, Zhang Y, Ross B, Lonka L, Takkunen E, Messer A, Sharp J, Wheeler R, Kusumi K, Mole S, Liu W, Soares MB, Bonaldo MF, Hirvasniemi A, de la Chapelle A, Gilliam TC, Lehesjoki AE. The neuronal ceroid lipofuscinoses in human EPMR and mnd mutant mice are associated with mutations in CLN8. Nat Genet. 1999; 23(2):233–236. [PubMed: 10508524]

Salek RM, Colebrooke RE, Macintosh R, Lynch PJ, Sweatman BC, Emson PC, Griffin JL. A metabolomic study of brain tissues from aged mice with low expression of the vesicular monoamine transporter 2 (VMAT2) gene. Neurochem Res. 2008; 33(2):292–300. [PubMed: 18041582]

Salek RM, Xia J, Innes A, Sweatman BC, Adalbert R, Randle S, McGowan E, Emson PC, Griffin JL. A metabolomic study of the CRND8 transgenic mouse model of Alzheimer's disease. Neurochem Int. 2010; 56(8):937–947. [PubMed: 20398713]

Sekhon SS, Maxwell DS. Ultrastructural changes in neurons of the spinal anterior horn of ageing mice with particular reference to the accumulation of lipofuscin pigment. J Neurocytol. 1974; 3(1):59–72. [PubMed: 4824789]

Trygg J, Wold S. Orthogonal projections to latent structures (O-PLS). J Chemometr. 2002; 16(3):119–128.

Wheeler RB, Sharp JD, Schultz RA, Joslin JM, Williams RE, Mole SE. The gene mutated in variant late-infantile neuronal ceroid lipofuscinosis (CLN6) and in nclf mutant mice encodes a novel predicted transmembrane protein. Am J Hum Genet. 2002; 70(2):537–542. [PubMed: 11727201]

Wold, S.; Albano, C.; Dunn, WJ.; Edlund, U.; Esbensen, K.; Geladi, P.; Hellberg, S.; Johansson, E.; Lindberg, W.; Sjöström, M. Multivariate data analysis in chemistry. Chemometrics: mathematics and statistics in chemistry. D. Reidel Publishing Company; Holland: 1984.

NIH-PA Author Manuscript

NIH-PA Author Manuscript

NIH-PA Author Manuscript

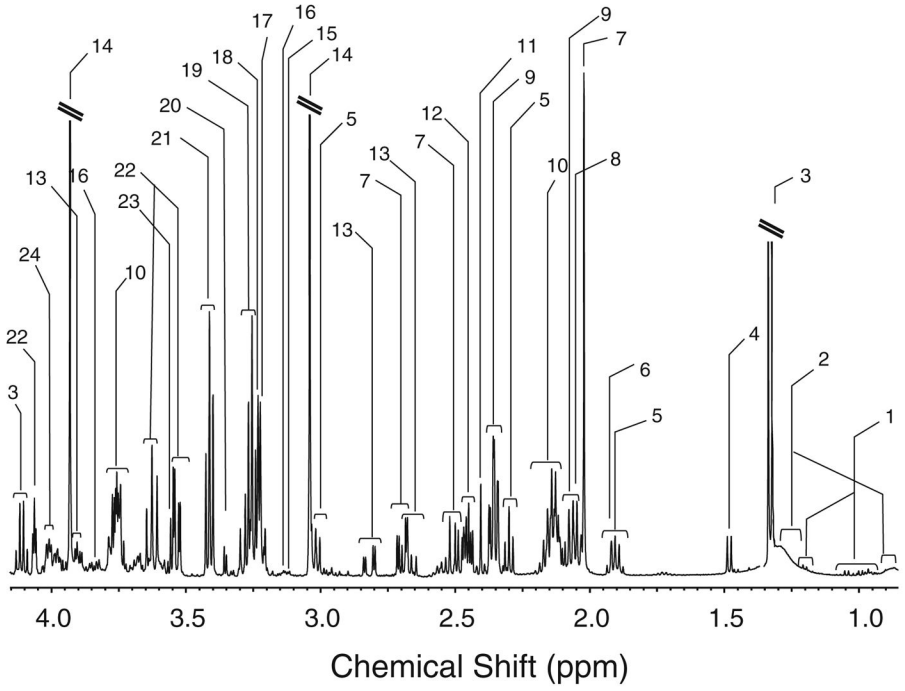

Fig. 1.

A high resolution solution ^{1}H NMR spectrum of an aqueous extract of cortex tissue taken from a *mnd* mice, recorded at a proton frequency of 500.13 MHz. *Peak 1*, valine, leucine, isoleucine; *peak 2*, fatty acids; *peak 3*, lactate; *peak 4*, alanine; *peak 5*, γ-amino butyric acid (GABA); *peak 6*, acetate; *peak 7*, N-acetyl-L-aspartate (NAA); *peak 8*, N-acetyl-aspartyl-glutamate (NAAG); *peak 9*, glutamate; *peak 10*, glutamate and glutamine; *peak 11*, glutamine; *peak 12*, succinate; *peak 13*, aspartate; *peak 14*, phospho-creatine; *peak 15*, malonate; *peak 16*, ethanolamine; *peak 17*, choline; *peak 18*, phosphocholine; *peak 19*, taurine and *myo*-inositol; *peak 20*, *scyllo*-inositol; *peak 21*, taurine; *peak 22*, *myo*-inositol; *peak 23*, glycine *peak 24* phosphoethanolamine

NIH-PA Author Manuscript
NIH-PA Author Manuscript
NIH-PA Author Manuscript

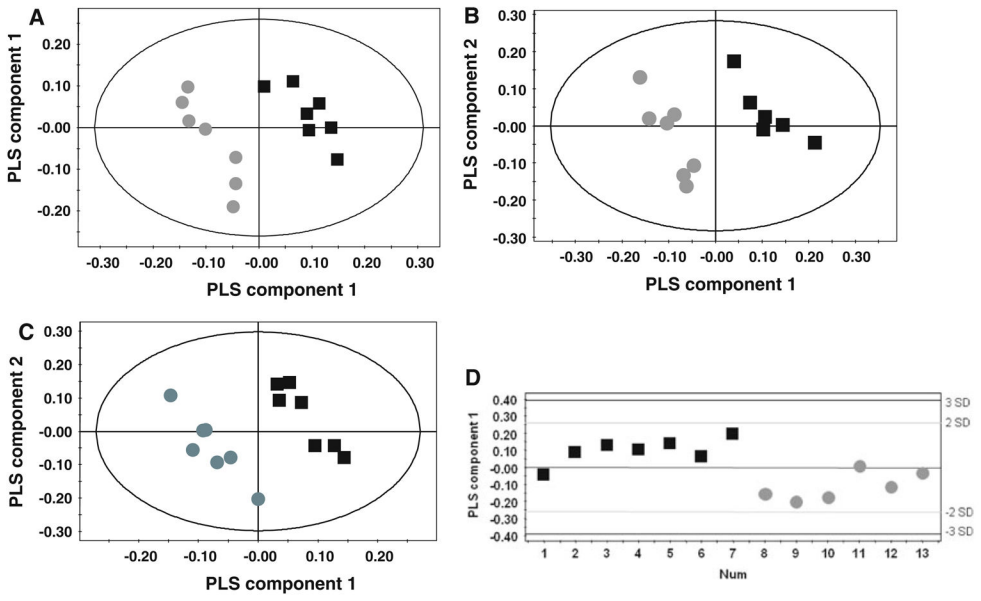

Fig. 2.

Pattern recognition models of metabolic changes identified in the brains of *mnd*, *nclf* and wildtype mice. PLS-DA score plots distinguishing wildtype (*black square*) and *mnd* (*dark grey circle*) ^{1}H NMR metabolic profiles derived from **a** the cortex [R^2Y = 98%; Q^2 = 77%], and **b** cerebellum [R^2Y = 95%; Q^2 = 68%]. Two components used for each model. PLS-DA score plots distinguishing wildtype (*black square*) and *nclf* (*dark grey circle*) ^{1}H NMR metabolic profiles derived from **c** cortex [R^2Y = 97%; Q^2 = 78%] using two component and **d** cerebellum brain tissue [R^2Y = 67%; Q^2 = 33%], one component

NIH-PA Author Manuscript
NIH-PA Author Manuscript
NIH-PA Author Manuscript

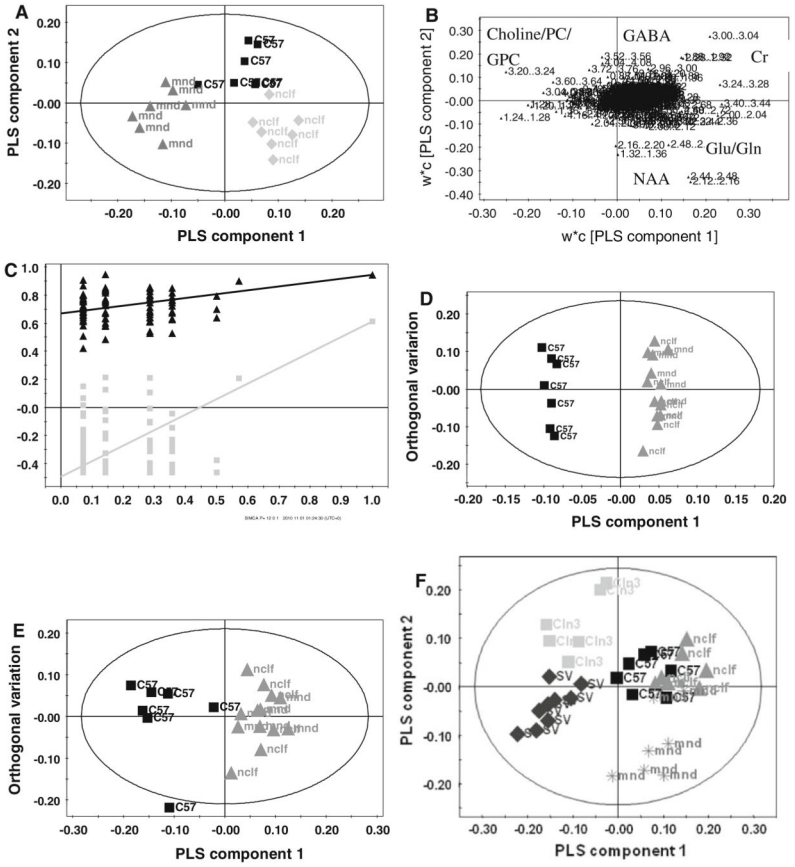

Fig. 3.

Comparison of different mouse models of NCL. **a** PLS-DA of ^{1}H NMR profiles derived from the cortex of wildtype (*black square*), *mnd* (*grey triangle*) and *nclf* (*light grey diamond*) mice [R^2Y = 95%; Q^2 = 69%] using 4 components. **b** The relevant loading plot, with important metabolites for classification highlighted and **c** the validation plot for model **(a)** as an example, assessing validity and the degree of overfit for the model. The validation plot for the first PLS-DA component of the PLS-DA model in A is shown. The validation plot displays the correlation coefficient between the original classification variables (Y-matrix) and the randomly permuted classification variables versus the cumulative R^2(*black triangle*) and Q^2(*light grey square*) for these models and draws the regression line. The intercept is a measure of the over fit. **d** An OPLS-DA score plot from cortex brain region separating the NCL mice model (*dark grey triangle* mnd and *dark grey triangle* nclf) from control mice (*black square*)[R^2Y = 98%; Q^2 = 67%] **e** OPLS-DA score plot separating the cerebellum of NLC mutants (*dark grey triangle* mnd and *dark grey triangle* nclf) from the wildtype (*black square*)[R^2Y = 85%; Q^2 = 38%]. **f** PLS-DA score plot of ^{1}H NMR profiles derived from the cortex of wildtype—c57 background (*black square*), wildtype—sv 129 (SV-*black diamond*) *mnd* (*dark grey asterisks*), *nclf* (*dark grey triangle*) and *Cln3* (*light grey square*) mice [R^2Y = 40%; Q^2 = 30%] using 2 components

NIH-PA Author Manuscript
NIH-PA Author Manuscript
NIH-PA Author Manuscript

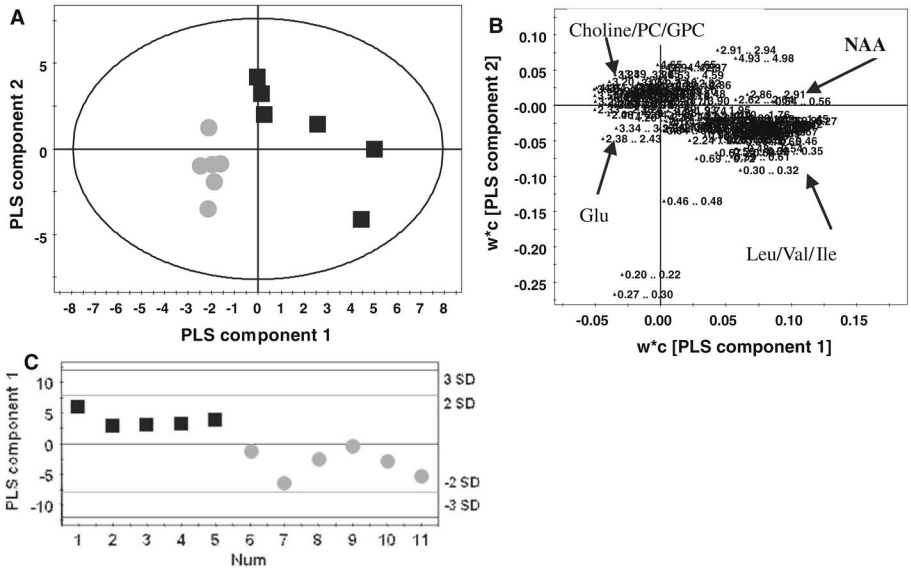

Fig. 4.

a PLS-DA score plot separating the cortex of the 19 month control mice (*black square*) from the (*dark grey circle*) 18 months *nclf* mice [$R^2Y = 61\%$; $Q^2 = 47\%$] **b** The relevant loadings plot for model **a** with important metabolites for classification highlighted. **c** PLS-DA of ^1H NMR profiles derived from the cerebellum of wildtype (*black square*) and *nclf* (*dark grey circle*) mice [$R^2Y = 79\%$; $Q^2 = 63\%$]

NIH-PA Author Manuscript

NIH-PA Author Manuscript

NIH-PA Author Manuscript

Table 1

mnd and *nclf* brain tissues phenotyped by metabolomic analyses

Genotype	Age (months)	*n* number
C57BL/6J control	6	7
	9	4
	19	6
mnd	6	7
nclf	6	8
	9	4
	18	6

Tissues are defined by age and *n* number

NIH-PA Author Manuscript

NIH-PA Author Manuscript

NIH-PA Author Manuscript

Table 2

Metabolic changes detected by multivariate data analysis in *mnd* and *nclf* cerebral tissue

Tissue	Relative increase in *mnd*	Relative decrease in *mnd*
Cortex	Choline/PC	Creatine
	GPC	GABA
	Lactate	Taurine
	Glutamine	NAA
	Glutamate	Aspartate
	Ethanolamine	*Myo*-inositol
	Isoleucine/valine/leucine	
	Scyllo-inositol	
Cerebellum	Lactate	Creatine
	Choline	Taurine
	PC and GPC	Glutamate
	Glutamine	*Myo*-inositol
		GABA

	Relative increase in *nclf*	Relative decrease in *nclf*
Cortex (1 and 6 month)	Glutamate	Choline/PC
	Glutamine (less)	Creatine
	NAA	*Myo*-inositol
	Asp	GABA
	Succinate	GPC
Cerebellum (1 and 6 month)	Lactate	Creatine
	Glutamine	*Myo*-inositol
	Asp	GABA
		Choline/PC
		GPC
		Glutamate
		Taurine
Cortex (18 month)	Choline/PC	Glutamine
	GPC	Lys-Leu/Ile-Val
	Glutamate	
Cerebellum (18 month)	Taurine	Choline/PC
	Glutamate	GPC
	Lys-Leu/Ile-Val	*Myo*-inositol
		GABA
		NAA
		Asp
		Creatine

Changes are listed for each of the brain regions examined. For the *nclf* mice there are two age groups of young (6 months) and older mice (18 months)

NIH-PA Author Manuscript

NIH-PA Author Manuscript

NIH-PA Author Manuscript

Table 3

Metabolic changes for GABA, NAA, glutamate and glutamine represented as ratios from the NMR spectra for the cortex brain region without any overlapping peaks

	C57 vs. *mnd*	C57 vs. *nclf*	129 vs. *Cln3* young	129 vs. *Cln3* old
GABA/Glu	$\uparrow^{0.04}$	–	–	$\uparrow^{0.05}$
Gln/Glu	$\downarrow^{0.03}$	$\downarrow^{0.05}$	$\downarrow^{0.002}$	$\downarrow^{0.02}$
NAA/Glu	$\uparrow^{0.008}$	–	–	$\uparrow^{0.05}$

A Student *t* test was carried out to determine the significance of the changes (reported for significant changes)